A turbines-module adapted to the marine site for tidal farms layout optimization

M. Pucci, D. Bellafiore, S. Zanforlin, and A. Frangioni

Abstract—**In this work we propose a new methodology for tidal farm layout optimization. For the optimization process we adopt a simple Mixed Integer Quadratic Programming (MIQP) algorithm, coupled with a wake model. The algorithm has a discrete approach, hence we establish a priori the available turbine locations in a staggered configuration. The novelty lies in the staggered configuration adopted as input of the optimization process: the staggered grid is tailor made thinking to a particular ocean site of interest. Hence, the staggered grid will be found by means of geometrical and site dependent evaluations, in particular by considering the range of prevalent flow directions characteristics of the site. In this way, we establish the best "module" made up of three turbines, which will be the building block of the staggered grid. This will allow us to adapt the algorithm to changing site, and at the same time to maintain it easy to implement, and quick in response thanks to the discrete approach. The application of this methodology to a case study farm made up of 9 machines, will show an increase in power production of about 6% compared to the power generated by the same number of devices optimized with a conventional staggered grid.**

Index Terms—**BEM, farm layout, HATT, MIQP, optimization, SHYFEM.**

I. Introduction

In recent years, the necessity of renewable energy generation systems is becoming more and more strategic, due to climate changes and geopolitical situations. In this framework, ocean energy plays an important role in clean energy production. Indeed, worldwide many companies are working on the development of tidal energy converters. Many developers have reached a Technology Readiness Level (TRL) of 7 and some of them have achieved the commercial level (i.e. TRL 9) [1]. In particular, this is true for Horizontal Axis Tidal Turbines (HATTs), which benefit of the wide know-how of the wind energy sector.

Since the sea and the ocean are subjected to interests of several stakeholders, from an energetic point of view it is essential to plan and design tidal farm by reaching the maximum power production. In this way, it is possible to reach higher power generation with equal sea surface exploited, or to reduce the sea surface with equal power output. In literature we can find many works which deal with farm layout optimization, especially in the wind field. One of the most adopted approach is to optimize the farm layout by using a Mixed Integer Quadratic Programming (MIQP) algorithm, or linearization of it (Mixed Integer Linear Programming, MILP) as in [2], [3], and [4] coupled with a wake model: the simplest and most popular wake model is the one proposed by Jensen [5].

The optimization process can be continuous or discrete: in the former the turbines locations can be varied with continuity in the horizontal space, whereas in the latter turbines can be placed only in the available locations, which are established a priori. To maintain the computation time of the optimization process low enough, it is necessary to adopt a discrete approach. But how to choose the available locations? Which is the best distancing between devices?

Many studies make some assumptions: for instance, it is necessary to leave 5 turbine diameters between devices in the flow direction, to grant a minimum wake recovery as explained in [6]; or a minimum technical distance must be kept between machines as in [7]. But, we find it necessary to adopt a set of available locations tailor made on the chosen marine site. The locations must be fixed taking into consideration the prevalent flow directions. In this work we will show some advantages to implement this strategy. We will compare two optimization processes: one performed using a conventional staggered grid as input of the optimization algorithm ($grid_1$ in the following), and one performed using a site-adapted grid ($grid_2$ in the following). Results are summarized as follows: in section II the methodology adopted is explained, in section III a case study is analysed, and some conclusions are provided in section IV.

II. Methodology

A. Structure of the optimization algorithm

In this work we adopt as optimization process a MIQP algorithm based on the Jensen's wake model for Horizontal Axis Turbines, which assumes a wake development described as follows:

Part of a special issue for EWTEC 2023. Original version published in EWTEC 2023 proceedings at https://doi.org/10.36688/ewtec-2023-416.

Manuscript submitted 20 December 2024; Accepted 8 January 2025. Published 31 May 2025.

This paper has been subjected to single-blind peer review by a minimum of two reviewers.

M. Pucci is with the Department of Energy, Systems, Territory and Constructions Engineering of the University of Pisa, 56122 Pisa, Italy (micol.pucci@phd.unipi.it).

D. Bellafiore is with the Institute of Marine Sciences-National Research Council (ISMAR-CNR), Castello 2737/F, 30122 Venice, Italy (debora.bellafiore@ve.ismar.cnr.it).

S. Zanforlin is with the Department of Energy, Systems, Territory and Constructions Engineering of the University of Pisa, 56122 Pisa, Italy (stefania.zanforlin@unipi.it).

A. Frangioni is with the Department of Informatics of the University of Pisa, 56122 Pisa, Italy (antonio.frangioni@unipi.it).

Digital Object Identifier: https://doi.org/10.36688/imej.8.83-90

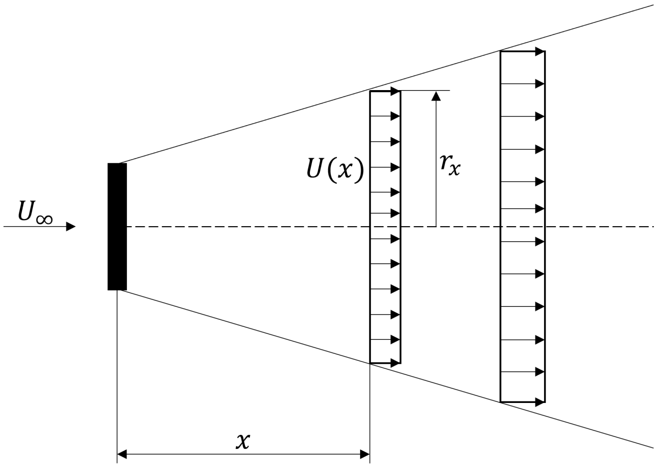

Fig. 1. Qualitative representation of the wake development in the Jensen's model.

$$U(x) = U_\infty \cdot [1 - d] \tag{1}$$

$$d = 2a \cdot (\frac{r}{r_x})^2 \tag{2}$$

$$r_x = \alpha x + r \tag{3}$$

where U_∞ is the undisturbed flow velocity, $U(x)$ is the wake velocity at a distance x downstream the turbine (the black rectangle in Fig.1), a is the axial induction factor imposed equal to 1/3, r is the turbine radius, and α determines the wake expansion and it is 0.035 (the reason of this value will be explained later on in this paper in section II-B). This is the basic formulation of the model: some improvements consist for instance in a gaussian shape velocity profile in wake, instead of a uniform profile, but this improvement will not be considered in this work. This wake model was born for wind turbines representation, but it can be extended to the tidal environment by tuning some parameters, as explained in [8]. The objective of the optimization is to maximize the power extraction: in other words, to minimize the wake interaction; hence, minimize the velocity deficit of the incoming flow on each turbine. Assuming N_t the number of turbine to place, p the number of available (discrete) locations, k a binary variable of dimension p, which will be equal to 1 if the p-th position is occupied by a turbine and 0 otherwise. Let be A a matrix pxp of the velocity deficit factor. The a_{ij} element of the matrix is equal to 0 if turbine i does not affect turbine j with its wake, otherwise a_{ij} represents the square of the wake velocity deficit and is found in analogy to what done in (2):

$$a_{ij} = d_{ij}^2 = (2a \cdot (\frac{r}{r_{xij}})^2)^2 \tag{4}$$

where r_{xij} is calculated as r_x, but using as x the distance between turbine i and j in the flow direction. To evaluate if turbine i is affecting turbine j with its wake, we have to assure the following condition:

$$y_{ij} \leq \alpha \cdot x_{ij} + r \tag{5}$$

where x_{ij} is the distance between turbines in the flow direction, whereas y_{ij} is the turbines transversal distance. If inequality (5) is verified, then turbine i is affecting turbine j. The procedure, which led to have a A matrix made up of a_{ij} elements, is widely explained in [2]. The optimization problem will become:

$$min(k^T \cdot A \cdot k) \tag{6}$$

$$k \in \{1, 0\} \tag{7}$$

$$\sum_{i=1}^{p} k(i) = N_t \tag{8}$$

B. Model test for a real-size turbine

The layout of the farm, which will result as output of the optimization process, will be tested using the SHYFM code, an Open Source Shallow Water equations software [9]. The SHYFEM code was equipped with a HATT model based on the Blade Element Momentum (BEM) theory, and will be used to compare several farm layouts. For this reason, we have to be sure that the SHYFEM turbine model correctly reproduces the fluid dynamics field all around the turbine. We had already tested and validated the model against experimental data for a prototype of 1 m diameter as explained in [10], but we want to assure that also a real size turbine is well captured from the model, in terms of performance and velocity field. Unfortunately, we have no available experimental data of a real size turbine. What we can do is to compare the results from the SHYFEM model to high fidelity CFD results. Hence, we consider as benchmark the real size turbine proposed in [11] and [12], which is geometrically similar to the one used in [10] for the prototype test, and also similar to the turbine used in the optimization process of this paper. The real size turbine has a 10 m diameter D_p, and the computational domain in [11] and in [12] is a rectangular parallelepiped $5D_p$ wide, $5D_p$ deep, and $40D_p$ long. The turbine is located $10D_p$ downstream from the inlet. The undisturbed flow velocity is 3.1 m/s. For our simulation we adopted the same aforementioned set up. Moreover, the grid resolution in turbine zone is 1/20 of D_p.

We first analyse the performance of the device, in terms of power coefficient C_P at different Tip Speed Ratios TSRs, defined as follows:

$$C_P = \frac{P}{1/2\rho A U_\infty^3} \tag{9}$$

$$TSR = \frac{r\Omega}{U_\infty} \tag{10}$$

where P is the produced power, ρ is the water density, A is the area swept by rotor's blades, and Ω is the rotational speed.

In Fig. 2 we can observe high fidelity CFD results from [12]: that work highlights how for high Reynolds numbers (order of magnitude 10^6), obtained by varying the turbine diameter or the undisturbed flow velocity,

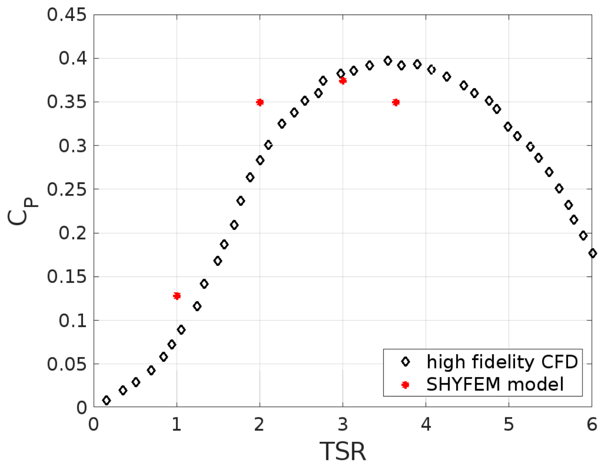

Fig. 2. C_P-TSR curve for a 10 m diameter turbine: comparison between the SHYFEM model (red asterisks) and the high fidelity CFD of [12] (black diamonds.)

the performance curve collapse into a single curve, which is the one shown in Fig. 2. SHYFEM results show a little underestimation of the maximum C_P, but also of the optimal TSR, 3 instead of 3.64.

For what concern the velocity field, and in particular the wake development, we compare our model with wake velocity profile of [11] from $1D_p$ to $15D_p$ downstream the turbine. The wake development in high fidelity CFD simulations is assured, since 160 turbine rotations were performed. In Fig. 3 we can observe good agreement between the two simulated turbines in the near wake and until $3D_p$ downstream. For the rest of the wake extension the SHYFEM model shows a faster recovery. However, also the behaviour of the far wake can be considered satisfying, seen the simplicity of the SHYFEM turbine model and the low computational time required for simulations (18 hours instead of 28 days of the high fidelity CFD). We wanted also to be sure that the Jensen's wake model correctly predicts the behaviour of a tidal turbine. Indeed, as already said, the Jensen's model was born for wind applications. However other works in literature have adopted this model with tidal turbines such as [13] and [8]. The latter makes a comparison between the Jensen's model predictions and CFD results, by adopting a wake expansion coefficient α equal to 0.04. We make an analogous evaluation by imposing α equal to 0.035. Fig.4 shows the good match between the Jensen's model prediction and the SHYFEM simulations results for what concern the center-line velocity recovery downstream the turbine. This fact is essential to a correct analysis, since we use the SHYFEM code to test the power production of the output configurations of the optimization process. This guarantees that differences in power generation of several optimized configurations are not due to a bad representation of the wake in the optimization algorithm.

C. Staggered grid choice

We find it necessary to choose an appropriate staggered grid as input of the algorithm, in order to maintain a simple and discrete optimization approach. The aforementioned grid should be fixed taking into consideration the site where we want to install the tidal farm. In particular, we want to chose the distances between the three turbines composing a module, that will be replicated to build the whole grid. Hence, we want to chose distances Δx and Δy between turbines T_1, T_2, and T_3 defined as in Fig. 5.

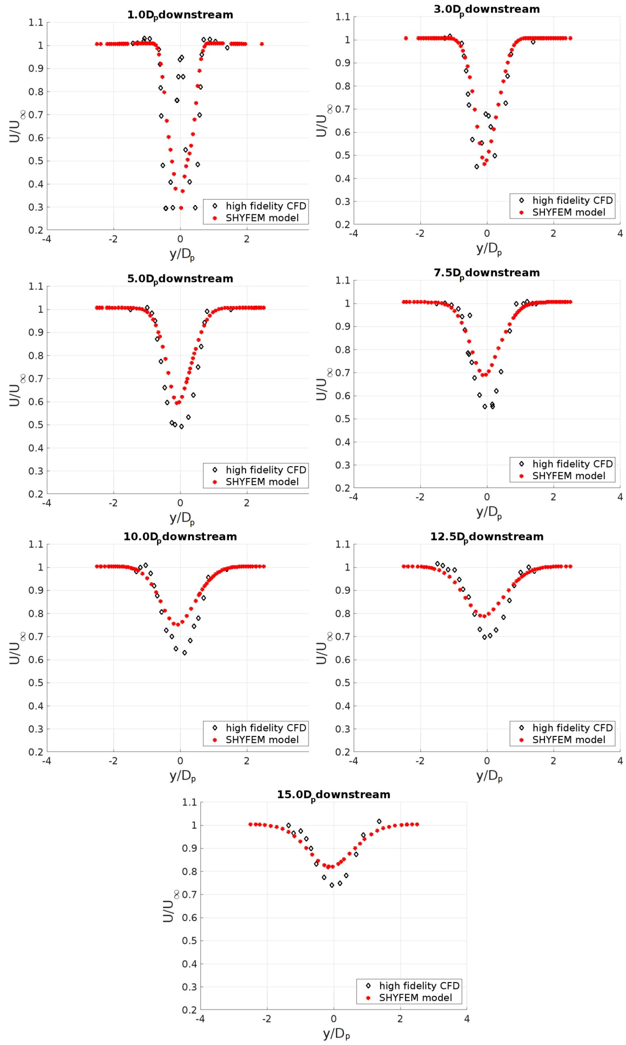

Fig. 3. Wake velocity profiles relative to the horizontal middle plane for a 10 m diameter turbine: comparison between the SHYFEM model (red asterisks) at the optimal TSR i.e. 3, and the high fidelity CFD of [11] (black diamonds) at the optimal TSR i.e. 3.64.

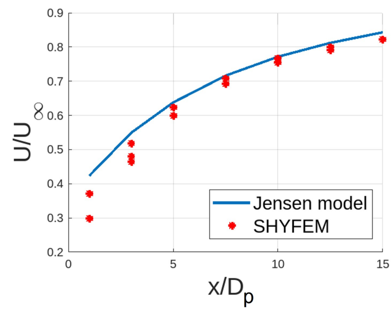

Fig. 4. Comparison between the wake center-line velocity deficit prediction of the Jensen analytical model (blue line), and the SHYFEM fluid dynamics simulations (red asterisks).

There are some examples of marine sites, which exhibit a flow inversion during a flood-ebb cycle which is nearly 180°. Some are localized in the Fromveur Strait [14], in Pentland Firth, off the coast near Orkney and near Pembroke as in [15], off the coast near Amlwch, the Bardsey Sound and the Ramsey Sound as in [16]. Hence, there are several sites which show a collection of velocity data with a rectilinear or elliptical shape, referring to a polar velocity graph: we can take as a qualitative example the one shown in Fig. 6, which represents the spread of velocity data as a function of the direction. Here we can see that even if the flood and ebb currents are not perfectly aligned, we can highlight a prevalent direction (black line in the figure), and take into consideration a tolerance range around this prevailing direction. In this way, we consider as exploitable flow velocity all those which fall within the tolerance angle, and consequently we adapt the three turbines module to these directions. In Fig. 5 we denote with θ the tolerance angle around the prevalent direction, i.e. direction 1. Hence, the flow can have a direction ranging between 2 and 3 as in figure. Once we have placed turbine T_1, we can establish distances Δx and Δy by geometrical evaluations: let's consider a flow coming from direction 3, and suppose that turbines have a control system able to regulate the yaw angle to the incoming flow. Hence, the turbines are perpendicular to the flow for each incoming directions. The shaded rectangle in Fig. 5 represents the wake of turbine T_1. Now, we have to chose the location of turbine T_2, and what we can observe is that Δx should respect the following constrain:

$$\Delta x \leq \frac{\Delta y}{tan(\theta)} - \frac{2r}{sin(\theta)} \tag{11}$$

This relationship represents the maximum distance Δx, which avoid wake interference among the three turbines in the module. Indeed, placing turbine T_2 at a Δx distance which underlies to (11), prevent wake interference for each incoming flow with directions ranging from 2 to 3. Moreover, we have fixed a minimum technical distance between the devices equal to 3 turbine diameters D_T (which falls in the range suggested by [7]). Hence, other constrains arouse:

$$\Delta y \geq 1.5 D_T \tag{12}$$

$$\Delta x \geq \begin{cases} 0 & \text{if } \Delta y \geq 1.5 D_T \\ \sqrt{(3D_T)^2 - \Delta y^2} & \text{if } \Delta y \leq 1.5 D_T \end{cases} \tag{13}$$

Equation (12) is necessary to impose the minimum technical distance between devices T_1 and T_3, whereas (13) imposes the minimum technical distance between turbines T_1 and T_2 (and symmetrically between turbines T_3 and T_2).

At this point, we have to decide the values for Δx and Δy. This will be done using an iterative process: we vary Δy from the minimum value (i.e. $1.5D_T$) to an arbitrary high value. Consequently, we calculate the constrains for Δx using (11) and (13). Not all the Δy will be feasible: indeed, some values can bring to unfeasible constrains for Δx. Hence, we chose the minimum feasible Δy available. This choice can be explain for two reasons: in theory Δy has no upper limit, hence we could enhance it to a huge value, but what we know from literature is that beneficial fluid dynamics effects between devices arouse if turbines are placed close enough. Moreover, a very high value for Δy will brig to a farm grid too large. Therefore, to maintain a reasonable farm extension, and to probably better exploit beneficial fluid dynamics mechanisms, we decided to fix Δy to the minimum available value. Once we established Δy, Δx can range between what prescribed in (11) and (13). The choice falls on the lower bound of Δx, i.e. (13). This can be explained referring to Fig. 7a). As it is built, the three turbines module has a triangular symmetry in direction 1. But, if we consider direction 3 (or 2 is irrelevant) we can note an asymmetry. If we denote with d_1 and d_2 the transversal distances between turbines (with a flow with direction 3) we can observe a relevant difference between d_1 and d_2. In Fig. 7b) it is highlighted how the more we approach T_2 towards the lower bound for Δx (the blue point in the figure), the more differences between d_1 and d_2 fade away. In other words, the turbine modules appears more symmetric also to direction 3 (and 2, which is specular). In this way, we assume a more fair treatment for the three directions considered, avoiding to privilege too much one direction instead of another.

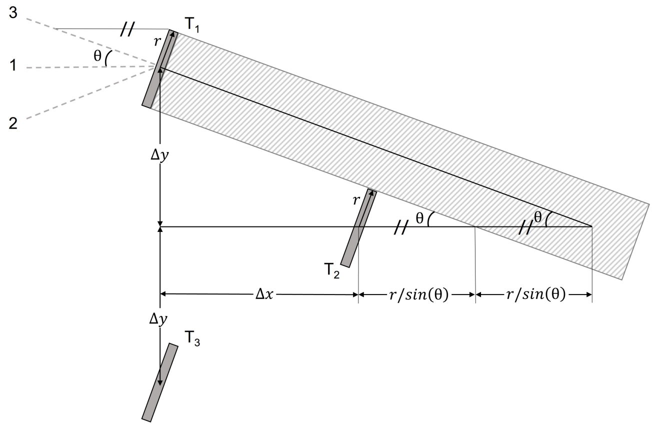

Fig. 5. Schematic representation of a three turbines module. The grey rectangles are turbines T_1, T_2, and T_3.

III. CASE STUDY

A. Site characterization and set up

As a case study we have considered the site called the Ramsey Sound, proposed in [17]: it is a strait located near St. David's headland, Wales, UK. It is 1500-1600 m wide, and about 3 km long with depth ranging between 20 m and 70 m. We consider the site characteristics for what concern velocity magnitude and directions. A measurement campaign was conducted as explained in [18], and it emerges that in the center of the Sound it can be approximately considered a bidirectional site, with a north-south dominant direction. Data collected during a flood-ebb cycle show a spread in velocity directions, but the more significant recorded velocities fall into a tolerance range of 20° with respect to the prevalent

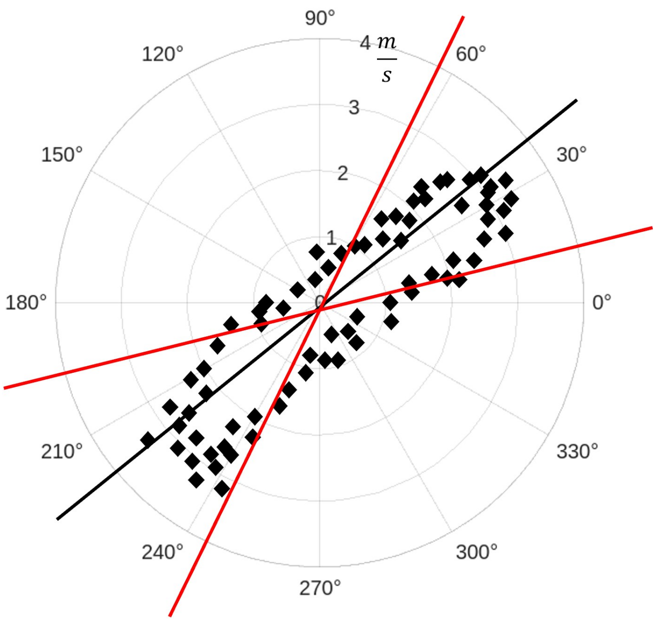

Fig. 6. Qualitative representation of velocity data spread in a site characterized by an elliptical polar graph. We can identify a prevalent direction (black line), and around it consider a tolerance range of directions bounded by the red lines, with suitable velocity for energy exploitation.

direction (north-south). This means velocities higher than 2 m/s during the flood tide with peaks of 4 m/s, whereas limited values during the ebb tide. Since, for this peculiar site the flood phase is the most relevant in terms of energy exploitation, we will focus our analysis only on flood phase. Therefore, as suggested in [17], an undisturbed flow velocity equal to 3 m/s can be considered to characterize the flood tide of the site. Hence, the latter velocity value will be the uniform inlet velocity for our optimization process, and consequently of our fluid dynamics simulations. The turbine considered has a diameter D_T of 18 m, and it is geometrically similar to the one used to test the real size model in section II-B.

We want to analyse the importance of the choice of the staggered grid given as input to a discrete optimization algorithm. Hence, we assign two different staggered grid as input: the one that we will call $grid_1$ has a Δy distance imposed equal to the minimum technical distance (i.e. $1.5D_T$), whereas Δx is imposed equal to $5D_T$ to grant enough wake recovery in analogy to what done in other works in literature, for instance [6] and [13]. The site-adapted grid, that we will call $grid_2$ is obtained following what explained in the previous section. The θ angle characteristic of the Ramsey Sound is 20°. The minimum feasible distance Δy is $2.5D_T$, and consequently Δx is imposed equal to the lower bound of $1.7D_T$.

We want to optimize the layout of a small farm made up of 9 devices. Both grids have a 6x6 configuration, hence 36 available locations. The layout outputs from the optimization algorithm are shown in Fig. 8. We can observe the locations available with different spacing between devices: in Fig. 8a) is represented the conventional grid with $3D_T$-$5D_T$ spacing, and in Fig. 8b) with $5D_T$-$1.7D_T$ spacing. The shaded rectangles

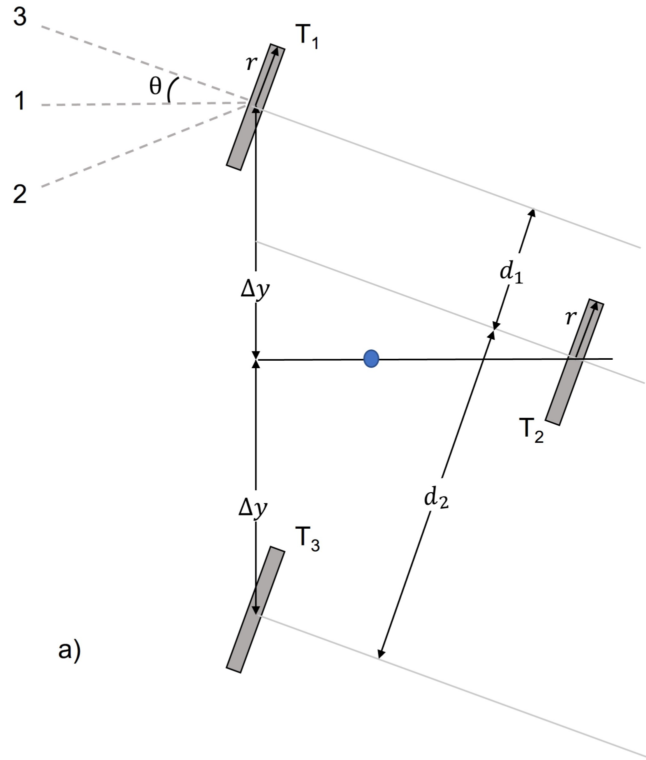

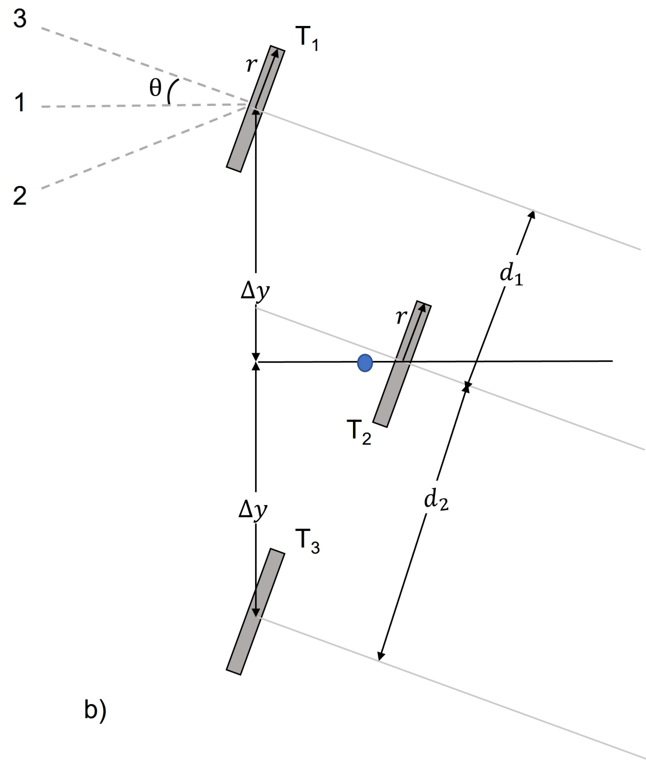

Fig. 7. a) shows the distances between T_1 and T_2 and between T_3 and T_2 perpendicular to the flow direction 3, which are respectively d_1 and d_2. b) shows how the difference in length between d_1 and d_2 can be mitigated by approaching turbine T_2 towards the lower bound for Δx, i.e. the blue point.

indicate the locations occupied by turbines. Now, we have to test the two different farm configurations with fluid dynamics BEM based simulations to attest which one is the best. The calculation domain has a depth of 70 m, and is $58D_T$ wide and $70D_T$ long in case of $grid_1$, whereas $70D_T$ wide and $50.2D_T$ long in case of

TABLE I

	$grid_1$	$grid_2$
P_{tot}	33.8 MW	35.8 MW
Power increment	/	+6%
A_{tot}	133650 m^2	15147 m^2
Power density	252.9 W/m^2	2363.5 W/m^2

Comparison between $grid_1$ and $grid_2$ farm in terms of total power production P_{tot}, and Power density.

$grid_2$. The grid horizontal resolution goes from 1 m in the turbine region to 40 m at the domain boundaries. The vertical discretization is equal to 1 m over the whole water column, and the turbines are centered in the middle of it. The undisturbed flow velocity is 3 m/s as already mentioned.

B. Results

We have simulated both farm configurations in three different flow directions: direction 1, which represents the prevalent direction, and direction 2 and 3, which are the extreme tolerance directions. All the velocity values with high energy content during flood tide, fall into the range delimited by direction 2 and 3. In Fig. 9 are proposed the flow fields for the three flow directions relative to $grid_1$, plotted on the middle horizontal plane. Analogous flow fields for $grid_2$ are shown in Fig. 10. This last configuration highlights the born of much more acceleration corridors between devices, and hence a more favorable flow condition. This is confirmed by Fig. 11 where the power outputs of the two farms are plotted: we can observe that the farm generated from $grid_2$ reaches higher power production for each of the three considered directions. Table I summarizes some data. The total power amount P_{tot}, defined as the sum of power generated at each direction, reaches an increment of about 6% in case of farm generated from $grid_2$. Moreover, let's consider the smallest rectangle able to contain the whole farm, the area of this rectangle is the total horizontal area A_{tot} occupied by the farm. We can observe a huge reduction in A_{tot} in case of farm obtained with $grid_2$. This will lead to an enormous increment in power density (defined as P_{tot}/A_{tot}), a nearly 10-times increase.

C. Sensitivity analysis

Since it is almost impossible to simulate an infinitely large domain for a farm, we want to assure that the extension of the domains used are large enough to prevent relevant blockage effects. The domains used to simulate $grid_1$ and $grid_2$ farms, where obtained by maintaining $20D_T$ of distance from the extreme points of the staggered grid. Considering Fig.8, we maintained $20D_T$ in direction North, South, East and West from the boundary location plotted in the grid.
To make a sensitivity analysis to the domain extension, we performed further simulations of the farm obtained with $grid_2$, considering only the flow direction 1. In this case, we enlarged the domain (in the direction perpendicular to the flow) of +10% and +20%, passing from a $70D_T$ wide domain, to a $77D_T$ and a $84D_T$ wide domain respectively.

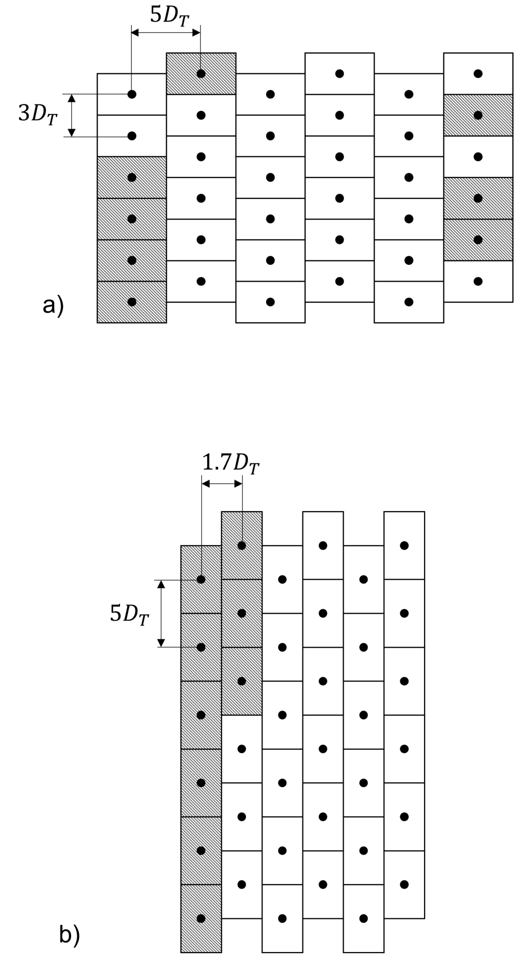

Fig. 8. a) $grid_1$ conventional staggered grid, and b) $grid_2$ site-adapted staggered grid. The shaded rectangles represent locations occupied by the 9 turbines of the cluster we wanted to optimize.

TABLE II
SENSITIVITY ANALYSIS

domain	Power	Δ %
+10%	12.16 MW	-0.78%
+20%	12.2 MW	-0.3%

Power outputs of the 9 turbines farm from the sensitivity analysis performed by enhancing the domain width. The Δ% column indicates the percentage difference in power outputs with respect to the original domain.

In Table II we can see the power outputs of the simulations: with Δ we denote the percentage difference in power output with respect to the original domain. Differences are negligible, hence we can conclude that the original chosen domains were large enough to avoid significant blockage effects.

IV. Conclusion

In this paper, we analysed the layout optimization of tidal turbines farms. Since, most of the works in this field make use of a discrete optimization algorithm to maintain low computational costs, we wanted to highlight the importance of the discretization choice.

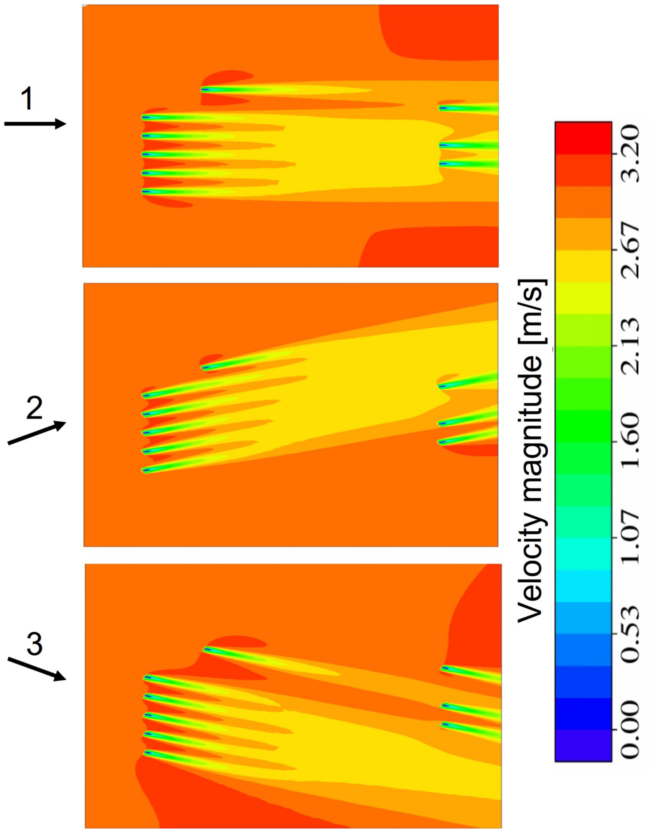

Fig. 9. $grid_1$ flow field of direction 1, 2, and 3. The flow fields are plotted on the horizontal middle plane.

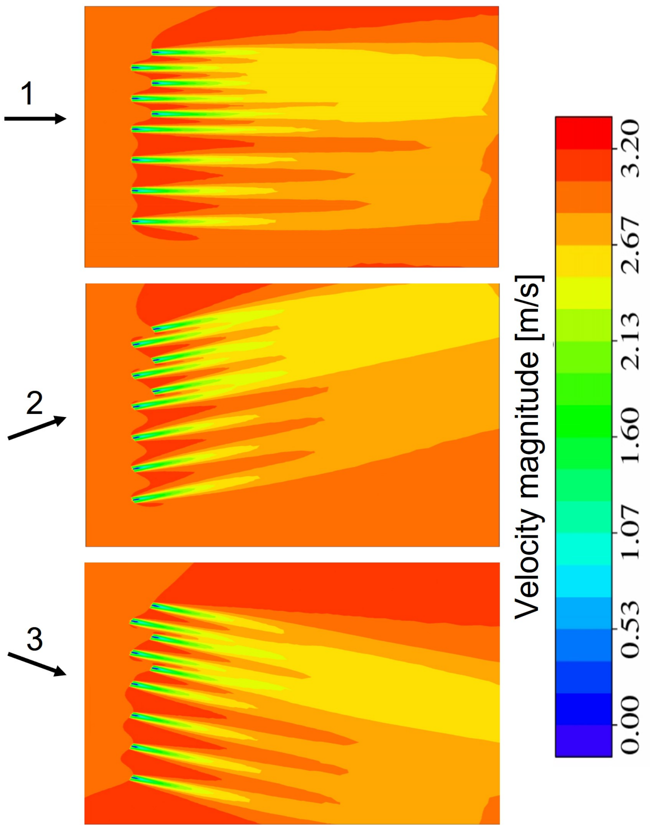

Fig. 10. $grid_2$ flow field of direction 1, 2, and 3. The flow fields are plotted on the horizontal middle plane.

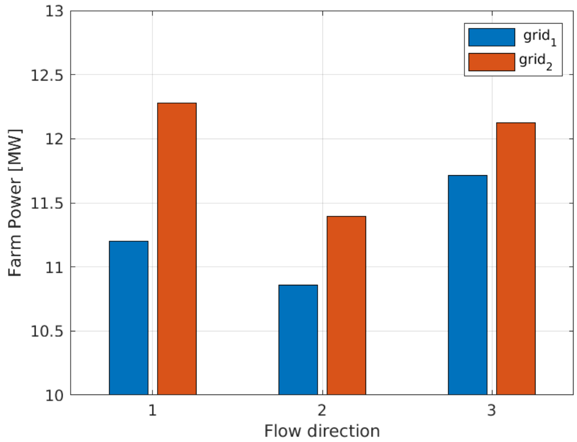

Fig. 11. Power amount of the 9 turbines farm for each flow direction.

Indeed, we have shown how a discretization only made by using literature assumptions (which was the $grid_1$ case in this paper), can be significantly improved. The tailor made discretization ($grid_2$) was built taking into consideration the flow characteristics of the site chosen for the farm installation. The module of three turbines replicated to build $grid_2$, was obtained from simple geometrical evaluations. Nonetheless, for a small cluster of 9 turbines, we have recorded an enhance in power production of 6% in case of the $grid_2$ farm, with respect to the $grid_1$ farm. Moreover, the power density (i.e. the ratio between the power production and the sea area occupied by the farm) has reached an augmentation of nearly 10 times. This is a not negligible result: indeed, a reduction in the sea area extension reserved for energy purposes, have positive repercussions from an environmental point of view, and also grant space for the other stakeholders activities.

Further development can be probably achieved, by making more complex fluid dynamics evaluations on the module of the three turbines. For instance, we can imagine to perform a set of fluid dynamic simulations to detect the best module configuration: in this case, we will also be able to better exploit favorable flow conditions in terms of a beneficial mutual influence among the turbines in the module.

References

[1] A. S. Sleiti, "Tidal power technology review with potential applications in gulf stream," *Renewable and Sustainable Energy Reviews*, vol. 69, pp. 435–441, 2017.

[2] S. D. O. Turner, D. A. Romero, P. Y. Zhang, C. H. Amon, and T. C. Y. Chan, "A new mathematical programming approach to optimize wind farm layouts," *Renewable Energy*, vol. 63, pp. 674–680, 2014. [Online]. Available: http://dx.doi.org/10.1016/j.renene.2013.10.023

[3] R. Archer, G. Nates, S. Donovan, and H. Waterer, "Wind Turbine Interference in a Wind Farm Layout Optimization Mixed Integer Linear Programming Mode," *Wind Engineering*, vol. 35, no. 2, pp. 165–178, 2011. [Online]. Available: https://doi.org/10.1260/0309-524X.35.2.165

[4] M. M. Aguayo, P. E. Fierro, R. A. De la Fuente, I. A. Sepúlveda, and D. M. Figueroa, "A mixed-integer programming methodology to design tidal current farms integrating both cost and benefits: A case study in the Chacao Channel, Chile," *Applied Energy*, vol. 294, 2021. [Online]. Available: https://doi.org/10.1016/j.apenergy.2021.116980

[5] N. O. Jensen, *A Note on Wind Generator Interaction*, D. Riso National Laboratory, DK-4000 Roskilde, Ed., 1983.

[6] R. Vennel, S. W. Funke, S. Draper, C. Stevens, and T. Divett, "Designing large arrays of tidal turbines: A synthesis and review," *Renewable and Sustainable Energy Reviews*, vol. 41, pp. 454–472, 2015. [Online]. Available: https://doi.org/10.1016/j.rser.2014.08.022

[7] S. Nasha and A. Phoenixa, "A review of the current understanding of the hydro-environmental impacts of energy removal by tidal turbines," *Renewable and Sustainable Energy Reviews*, vol. 80, p. 648–662, 2017. [Online]. Available: https://doi.org/10.1016/j.rser.2017.05.289

[8] C. H. Jo, J. H. Lee, Y. H. Rho, and K. H. Lee, "Performance analysis of a HAT tidal current turbine and wake flow characteristics," *Renewable Energy*, vol. 65, pp. 175–182, 2014. [Online]. Available: https://doi.org/10.1016/j.renene.2013.08.027

[9] [Online]. Available: https://github.com/SHYFEM-model/shyfem

[10] M. Pucci, C. Di Garbo, D. Bellafiore, S. Zanforlin, and G. Umgiesser, "A BEM-Based Model of a Horizontal Axis Tidal Turbine in the 3D Shallow Water Code SHYFEM," *J. Mar. Sci. Eng.*, vol. 10(12), 2022. [Online]. Available: https://doi.org/10.3390/jmse10121864

[11] S. Salunkhe, "Model- and full-scale predictions of hydrokinetic turbulent wake, including model-scale validation," 2016.

[12] A. Mason-Jones, D. M. O'Doherty, C. E. Morris, T. O'Doherty, C. B. Byrne, P. W. Prickett, R. Grosvenor, I. Owen, S. Tedds, and R. Poole, "Non-dimensional scaling of tidal stream turbines," *Energy*, vol. 44, pp. 820—-829, 2012. [Online]. Available: https://doi.org/10.1016/j.energy.2012.05.010

[13] O. A. Lo Brutto, J. Thiébot, S. S. Guillou, and H. Gualous, "A semi-analytic method to optimize tidal farm layouts – Application to the Alderney Race (Raz Blanchard), France," *Applied Energy*, vol. 183, pp. 1168–1180, 2016. [Online]. Available: https://doi.org/10.1016/j.apenergy.2016.09.059

[14] T. El Tawin, N. Guillou, J. Charpentier, and M. Benbouzid, "On Tidal Current Velocity Vector Time Series Prediction: A Comparative Study for a French High Tidal Energy Potential Site," *Journal of Marine Science and Engineering*, vol. 7, no. 46, 2019. [Online]. Available: https://doi.org/10.3390/jmse7020046

[15] M. Lewis, R. Hashemi, S. Neill, and P. Robins, "The direct effect of waves on the tidal stream energy resource." International Conference on Renewable Energies Offshore, Portugal, Lisbon, 2015, pp. 169–176.

[16] M. Piano, S. P. Neill, M. J. Lewis, P. E. Robins, M. R. Hashemi, A. G. Davies, S. L. Ward, and M. J. Roberts, "Tidal stream resource assessment uncertainty due to flow asymmetry and turbine yaw misalignment," *Renewable Energy*, vol. 114, pp. 1363–1375, 2017. [Online]. Available: https://doi.org/10.1016/j.renene.2017.05.023

[17] C. H. Frost, P. S. Evans, M. J. Harrold, A. Mason-Jones, T. O'Doherty, and D. M. O'Doherty, "The impact of axial flow misalignment on a tidal turbine," *Renewable Energy*, vol. 113, pp. 1333–1344, 2017. [Online]. Available: https://doi.org/10.1016/j.renene.2017.07.006

[18] P. Evans, A. Mason-Jones, C. Wilson, C. Wooldridge, T. O'Doherty, and D. O'Doherty, "Constraints on extractable power from energetic tidal straits," *Renewable Energy*, vol. 81, pp. 707–722, 2015. [Online]. Available: https://doi.org/10.1016/j.renene.2015.03.085